neoDavid

A Humanoid Robot With Variable-Stiffness Actuation and Dexterous Manipulation Skills

By Sebastian Wolf, Thomas Bahls, Bastian Deutschmann, Alexander Dietrich, Marie Harder, Hannes Höppner, Cynthia Hofmann, Ana Huezo Martin, Manuel Keppler, Leonard Klüpfel, Henry Maurenbrecher, Xuming Meng, Anne E. Reichert, Manuel Stoiber, Markus Bihler, Maxime Chalon, Oliver Eiberger, Werner Friedl, Markus Grebenstein, Maged Iskandar, Viktor Langofer, Martin Pfanne, Antonin Raffin, Jens Reinecke, Tilo Wüsthoff, and Alin Albu-Schäffer

Dexterity and strength are essential for performing a variety of tasks in the unstructured environments of household services and craftsmanship. For these tasks, we have developed neoDavid, a robust humanoid robot with dexterous manipulation skills. neoDavid has joints with variable stiffness actuators (VSAs), which have mechanically adjustable elasticity in the drive train, a continuum elastic neck, and a gravitationally compensated torso with overload couplings. We present our modular approach in the development, starting from system architecture over mechatronic components, communication, and control to higher-level software. We demonstrate how this modularity enables scalable enhancements, allowing us to evolve the system from a single arm and hand into a complete humanoid robot. Additionally, we highlight advancements in perception, manipulation, and motion planning, along with the implementation of offline task planning utilizing capability maps. The versatile character in terms of dexterity and robustness is demonstrated in challenging applications, e.g., handling a drill hammer, fine manipulation of a pipette, and emptying a dishwasher.

Digital Object Identifier 10.1109/MRA.2025.3599706

INTRODUCTION

MOTIVATION

The underlying idea of the neoDavid (Figure 1) development, initially called the *DLR Hand Arm System* [1], is based on the fundamental observation that collisions with the environment, whether intentional or unintentional, are essential aspects in application scenarios where humans and robots share the same physical space. Unintentional contacts may arise from errors in task execution, inaccuracies in environmental models, or during learning-from-failure processes where collisions are an inherent aspect of the process. Conversely, a wide variety of tasks deliberately involve physical interactions and collisions, such as those found in service robotics, craftsmanship, or manufacturing settings. In these contexts, the robotic hand is of great importance. It is often the most vulnerable and exposed component, yet it also has to withstand the full load of dynamic movements and collisions [2]. As a result, one of the main driving factors in the design of neoDavid is robustness against collisions. Moreover, since the environment in which humanoid robots will operate in the future has been originally designed for humans, it is naturally advantageous to design such systems with human-like size, performance, and kinematics.

STATE OF THE ART

The landscape of compliant humanoid robots encompasses a diverse range of systems, featuring various forms of compliance. Table 1 gives an exemplary overview of those systems, which are, in our opinion, particularly commendable for their contributions to the advancement of compliant humanoids. COMAN [4], [5], evolved from iCub and cCub, integrates torque sensors and elastic actuators for safe interactions with people and objects, even during collisions, aiming for advanced manipulation and locomotion. WALK-MAN [6], [7], tailored for disaster recovery, excels in heavy lifting and navigating debris, equipped for dexterous tasks and durable movement. Both employ serial elastic actuators (SEAs) for smooth motions, with COMAN focusing on safe close interactions, and WALK-MAN addressing emergency scenarios' demands. The fascinating mechanical design of LIMS2-AMBIDEX [10] emphasizes a lightweight structure with minimal moving mass, leveraging cable-driven actuators for precise and high-speed manipulations. Among these innovative designs, ALTER-EGO [9] uniquely employs VSA [12] technology to intrinsically vary stiffness, offering enhanced interaction safety and adaptability. Musashi [11] features highly integrated SEA modules connected to a skeletal structure by tendons. Motion is primarily generated by learning control systems. It has underactuated 30-degree-of-freedom (DoF) hands with eight motors each. Several articulated tendon-driven elastic robotic hands have been designed in an effort to mimic how humans adjust hand compliance through tendon control. Notable examples include Shadow hand [13], UB Hand III [14], the three-fingered hand by Ozawa et al. [15], and Pisa/IIT SoftHand [8].

Robots and robotic hands mentioned earlier have been designed with compliance, but they have not yet been combined into a single humanoid robot capable of providing both mechanical robustness and dexterous manipulation in a human-sized form. The humanoid system neoDavid, equipped with an upper body with a similar number of DoF as humans, pushes the functional boundaries further by allowing stiffness adjustments for each of the joints of its upper extremities, suggesting a new horizon in functional versatility and managing complexity of humanoids.

OBJECTIVES

To develop a humanoid that operates dexterously and robustly in service tasks and craftsmanship, the following requirements must be met:

- *Human appearance*: In terms of accessibility of human and domestic surroundings, all mechatronic components, including mechanics, actuators, sensors, power, and communication electronics, have to be integrated in an anthropomorphic human-like appearance.
- *Modularity in the system architecture*: All components integrated in neoDavid shall be as modular as possible, such that gradual extensions and modifications are implementable and the high overall level of system complexity is manageable in a structured way.
- *Robustness against impacts*: To withstand even severe impacts, the mechanics have to be designed accordingly, involving intrinsically elastic and adaptable actuation principles.
- *Fast and powerful interaction with tools*: Robust and powerful components should be integrated into the system to enable the use of power tools weighing 1 kg or more.

DLR, CC-BY 3.0

FIGURE 1. The dexterous humanoid neoDavid is assembled of the elastic upper body David and the four-wheeled omnidirectional mobile platform NEO.

- *Fine manipulation of tools and objects*: The ambitious goal is to challenge the variety of human tools from fine manipulation with the need for grasp transition and in-hand manipulation to power-tool usage in one single system. Such skills require accurate mechanics, perception, control, planning, and high finger dexterity.

This article is structured as follows. After the system overview in the "System Architecture" section, the subareas of mechatronics (see the "Mechatronics" section), control (see the "Motion and Interaction Control" section), perception (see the "Perception" section), and manipulation (see the "Manipulation" section) are introduced individually, emphasizing their individual contributions to neoDavid. The "Validation and Discussion" section presents experimental demonstrations on the robot that illustrate the joint action of all involved components. In the final section we present our conclusion and future work.

SYSTEM ARCHITECTURE

The anthropomorphic lightweight system neoDavid is a research robot designed to solve complex manipulation tasks in unstructured environments. As such, the depth of development ranges from mechatronics to skills to applications as well as interaction with a human. To give an overview of the involved topics and communication structure, we classified these in system architecture layers, shown in Figure 2. We distinguish among

- *task-planning layer* intended for scheduling, high-level task priority handling, and human-robot interaction
- *executive layer* in which we develop our applications and coordinate the skills
- *behavioral control layer* with skills that are needed to fulfill a task as well as low-level data processing software
- *mechatronics layer* which is the lowest level, including the physical manifestation as well as firmware and middleware for communication.

Software in the task-planning layer with automatic scheduling or high-level task priority handling will be the next big step for autonomy on neoDavid. Currently, we rely on human input over graphical user interfaces, buttons, and physical human-robot interaction (pHRI).

Software modules are connected via the so-called *Links and Nodes* framework is a DLR system deployment software similar to Robotic Operating System (ROS)/ROS2. It aims at providing a clear view of the running modules (viewer, Simulink, and vision processing) and the way they exchange data. It provides software topic publisher/subscriber and service provider/client communication.

The main research activities are on the mechatronics and skills level, as indicated in orange in Figure 2. Our development philosophy emphasizes a holistic approach to research and development, ensuring that individual advancements are reliable, compatible, and integrate seamlessly into the larger system. This prevents new features or technologies from degrading overall system performance. By aligning our research goals with practical applications, we focus on

TABLE 1. An overview of compliant humanoid robots.

ROBOT (YEAR)	DEVELOPER	MAIN FEATURES	HEIGHT	WEIGHT	ACTIVE DOF (UNDERACTUATED DOF)	APPLICATION AREAS
neoDavid (2023)	DLR	VSA upper body, 20 DoF hand, ESP tracking control, dexterous manipulation	1.76 m	218 kg	52 [7/right arm, 5/left arm, 20/right hand, 6/left hand, 3/torso, 3/neck, 8/platform]	Household and craftsmanship tasks
Rollin' Justin [3] (2009)	DLR	Torque-controlled, whole-body compliance control, autonomous	1.91 m	200 kg	51 [7/arm, 12/hand, 3/torso, 2/neck]	Household tasks, astronaut assistance
COMAN [4], [5] (2013)	IIT	Torque-controlled, whole-body compliance control; key joints with SEA	0.95 m	31.2 kg	31 [6/leg, 7/arm, 3/torso, 2/neck]	Human-robot interaction, uneven terrain
WALK-MAN [6], [7] (2018)	IIT, University of Pisa	Advanced SEA, dexterous manipulation	1.92 m	132 kg	33 (69) [6/leg, 7/arm, 3/torso, 2/neck, 1 (19)/PISA/IIT SoftHand] [8]	Disaster response
ALTER-EGO [9] (2019)	IIT, University of Pisa	VSA technology, anthropomorphic upper body, self-balancing mobile base	1.00 m	21 kg	16 (52) [2/base, 5/arm, 2/neck, 1 (19)/PISA/IIT SoftHand [8]	Physical human-robot interaction and teleoperation (e.g., Avatar Xprize)
LIMS2-AMBIDEX [10] (2018)	KOREA-TECH	Lightweight arms with low moving mass (2.63 kg) for high-speed manipulation	N/A	N/A	19 [7/arm, 1/gripper, 3/neck]	Manipulation of foldable objects
Musashi [11] (2019)	JSK, IMI, University of Tokyo	Musculoskeletal humanoid with component modularization	1.59 m	40.1 kg	52 (96) [7/arm, 8 (30)/hand, 8/leg, 3/torso, 3/neck]	Understand muscle systems and mechanisms in the human body, real-world task execution

N/A: not available.

delivering tangible real-world value. This approach directs our efforts toward making a meaningful impact, rather than simply pursuing theoretical advancements. As a result, our research becomes more relevant and useful within the broader research context, ultimately driving more significant contributions to the field.

RESEARCH FOCUS ON SUBSYSTEMS

The constraints in size and shape, as well as the various research goals on neoDavid, require a well-structured system architecture. It also helps to tell apart system components to be improved through research from commercial off-the-shelf (COTS) elements. As is generally known, the mechatronic layer of a robot consists of sensors, actuators, motor current controls, and enabling subsystems. The research fields on neoDavid are focused on the highly integrated and compact lightweight subsystems related to

- sensors
- actuators
- internal communication between computers, actuators, and sensors
- heat management, including water cooling

while reliable COTS components are used for

- power supply as an enabling subsystem
- computers as a part of the control subsystem
- a local area network (LAN) for communication between the computers, which is part of the control subsystem
- the four-wheeled mobile platform.

During the system design and development process, the selection of system elements, assemblies, and even single hardware parts and materials is based on this differentiation. A special challenge for the selection is to solve the conflict between using special components for highly integrated compact subsystems and following a reasonable modular approach to reuse parts.

MODULAR APPROACH

To effectively manage complexity, we employ a modular design approach that integrates hardware, control firmware, and a flexible communication infrastructure. This involves dividing the system into smaller independent modules that can be developed, tested, and optimized separately and then integrated into the larger system. Our modular concept enables greater flexibility, expandability, and ease of technology transfer between robots while also simplifying the creation of test beds.

MECHATRONICS

With neoDavid, we have made a paradigm shift in the mechatronic technology of the robots at DLR from torque-sensor-based actuators to macroscopic elasticity in VSA. We

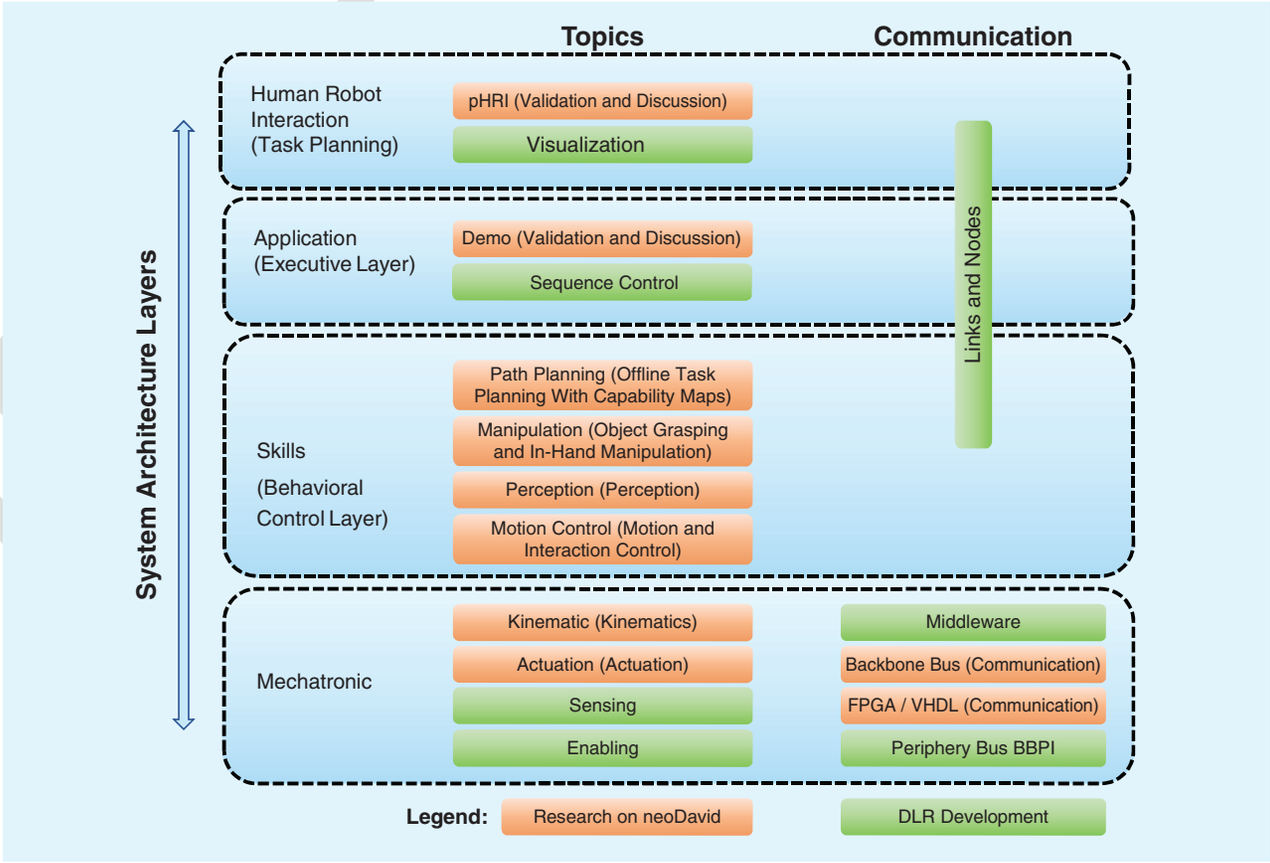

FIGURE 2. neoDavid's system architecture and research fields (small boxes) of the four system architecture layers. The section titles of the sections that provide more detailed information on each area of research are given in parentheses.

faced significant challenges in manifesting this new technology, particularly in terms of achieving the required high integration density in a humanoid form. The mechatronic development of neoDavid focuses on the upper body, designated as David. The lower body of neoDavid, designated as NEO, incorporates the mobile platform MPO-700, developed by Neobotix GmbH, along with the battery, real-time PC, application PC, and power supplies. For the sake of simplicity, the following mechatronic sections will focus on the upper body, including the figures.

KINEMATICS

The initial version of the robot, designated as the DLR Hand Arm System [1], has been built as one right arm with 7 DoF and one right hand with 19 DoF. While working with the robot in various setups and more demanding service and craftsmanship applications, such as the use of a hammer or fine manipulation with a pipette, the size of the workspace in front of the body became increasingly important.

Now, neoDavid has two arms and an active torso with 3 DoF to address the need to increase the capability map area; see the "Offline Task Planning With Capability Maps" section. The upper-body David weighs 55 kg and has a total of 44 DoF, as shown in Figure 3. The mobile platform NEO weighs 163 kg with four wheels and 8 DoF for omnidirectional driving. For two-handed manipulation of objects, an overlap of capability maps of the two arms is beneficial, but this is at the cost of the overall size of the reachable area. For the creation of a well-balanced overlap of the capability maps of the two arms in front of the body, the first shoulder axis is not pointing orthogonal sidewards but points more to the front and upwards. Both angle inclinations also help to bring the intersection points of the three shoulder axes of the arms closer together. This results in a more human-like appearance with a smaller shoulder width. Furthermore, the motion range of 205° in the floating spring joint (FSJ) [16] is upgraded to a motion range of 271° and integrated in both arms.

The hand has been upgraded from Dyneema tendons and friction bearings to steel tendons and ball bearings. This has resulted in significant improvements in modeling and friction [17]. Ring and little finger tendon routings are now modified to remove position couplings, leaving only stiffness couplings in the proximal interphalangeal and distal interphalangeal joints. The metacarpal rotation in the little finger has been discarded because the benefit of this joint has turned out to be insignificant. The thumb kinematics is changed to match the other fingers for simpler maintenance. Furthermore, by increasing the pulley diameters, the thumb got stronger. However, the latter change came along with some sacrifice in terms of motion range.

The left forearm and hand have a reduced design to decrease complexity with fewer motors and parts and also to test the technology with simpler kinematics. The forearm features no wrist joints, resulting in a 5 DoF left-arm kinematics. The left hand has only two identical opposing fingers (each 4 DoF) with the kinematics of a middle finger of the right hand.

ACTUATION

To handle the large number of drives integrated in the system, a generic and modular approach regarding hardware and control firmware is pursued. Due to requirements such as low inertia, high dynamics, and small form factors with high torque, permanent magnet synchronous motors (PMSMs) are

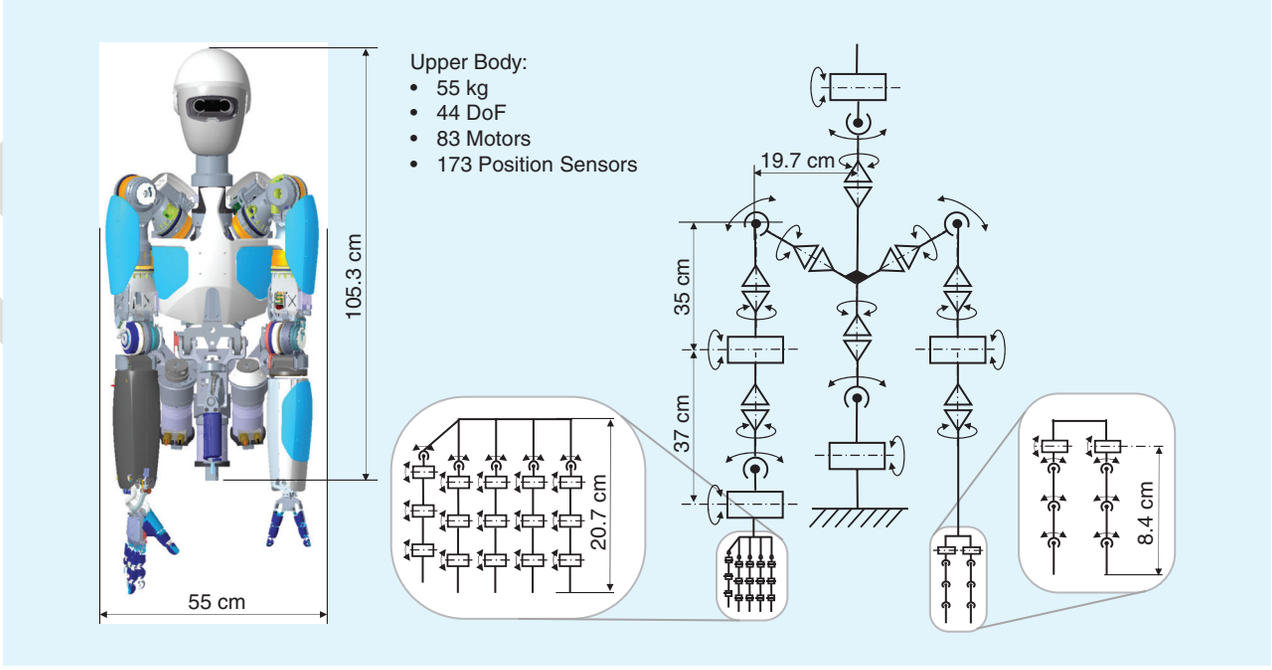

FIGURE 3. A representation of the upper-body kinematics of neoDavid in a simplified view. The right five-finger hand and the left two-finger hand are shown in enlarged form. The locations of the VSAs are indicated on the example of the right arm and hand.

almost exclusively deployed. A field-oriented control algorithm is used and implemented in field-programmable gate arrays (FPGAs) to provide the required control bandwidth with a current control frequency of 100 kHz [1]. To verify any changes to the motor control firmware before applying it to the hardware, a floating-point VHDL PMSM simulation model is used to complement the firmware.

ELECTRONIC MODULES

The digital inverter electronics stack is an integrated module consisting of a base power supply module and up to eight stackable smart inverter modules. The power supply contains the dc/dc converters, and each smart inverter module contains a three-phase voltage source inverter as well as a digital electronics part with a Xilinx Virtex 5 FPGA. The FPGA comprises the motor control firmware module as well as the sensor communication and SpaceWire backbone communication interface.

MOTOR MODULES

neoDavid utilizes four types of motor modules. In the torso are TQ-Robodrive ILM70x18 commuted with RD70 position sensors. The main motors in the arms are TQ-Robodrive ILM50x14 with a custom off-axis position sensor setup for a more compact design. A miniservo motor module based on the TQ-Robodrive ILM25 series was developed to satisfy the need for an integrated small form factor servo drive with high control bandwidth and high torque density. The module is used as a stiffness adjuster motor in the FSJ as well as the main drive in the forearm and used for finger actuation. A power electronics printed circuit board (PCB) with an integrated commutation sensor and an FPGA-based digital electronics PCB are directly mounted to the motor. The neck is driven by Robotis' Dynamixel MX servo drives.

FSJ

The FSJ is a modular and compact VSA unit with an integrated joint bearing. It is used in the three shoulder joints of each arm and in a special hinge joint version in both elbows; see Figure 4(a). The FSJ is based on an asymmetric actuation design, where one large motor (ILM50) is responsible for the output motion and one small motor (ILM25) changes the mechanical stiffness; see Table 2. The spring mechanism contains a single floating spring between two antagonistic cam disks.

Absolute position sensors with 16-bit resolution measure output position, passive deflection, and stiffness setup. Redundant information on the joint state is gathered together with the motor encoder positions, which are used for error detection and safety. The mechanism is designed to feature low friction and high structural stiffness to minimize unmodeled side effects, which could affect the system accuracy. The overall system performance is affected by mechanical losses due to friction torques in the drive train [18]. The Harmonic Drive (HD) gears dominate the frictional behavior, which varies with velocity, load, and temperature. Temperature sensors are integrated in the FSJ on the HD gearbox and motors.

BIDIRECTIONAL ANTAGONISTIC VARIABLE STIFFNESS ACTUATOR

This concept is an extension of an antagonistic actuator; see Figure 4(b). Two different bidirectional antagonistic variable stiffness (BAVS) implementations are developed for the wrist and forearm rotation [19]. All BAVS implementations have a symmetric actuation design with two equally sized ILM25 motor modules. In bidirectional mode, both motors can pull and push in each direction of the joint so that the individual maximum motor torques can be superimposed. Two identical antagonistic mechanisms with cam disks are located in series to the motors. The output stiffness is altered in the spring mechanism by spring preload and also by the changing gear ratio effect. Three different types of cam disks have been developed and tested for better practicability with an increased spring energy capacity and a wider area of stiffness setup. Absolute position sensors with 16-bit resolution measure the output position and the passive deflection.

TORSO

The torso system is composed of a tendon-driven base with 2 DoF to enable leaning to the front or the back and side-to-side motions [20] as well as a shoulder rotation joint with 1 DoF to allow for vertical rotation of the upper body. The base is actuated by three tendon actuators, and due to direct tendon routing using only one pulley along the tendon path, the tendon kinematics is nonlinear. The drive pulleys are fitted with overload couplings to prevent damage to the system and to protect against overloading caused by external impacts. Parallel to the actuation forces, a spring compensation system is implemented to counteract the majority of gravitational torques.

FLEXIBLE ANTAGONISTIC SPRING

The flexible antagonistic spring (FAS) (see [21]) is a variable-stiffness spring element for tendon-driven joints such as the neoDavid Awiwi hand, which is actuated in an antagonistic manner; see Figure 4(c). This technology is currently employed in the third-generation neoDavid hand as well as the two-fingered left hand. The antagonistic setup can apply a tendon preload, compensate for the nonlinear wrist transmission, and allow dislocation of the joint during hard impacts. For a robot hand, which is designed to operate in unstructured and partly unknown environments, this capability can be essential.

The FAS is located in the tendon path between the motor and the finger. To fit to the 20 different joints of the right hand and 38 different tendon lengths, which affect the stiffness behavior strongly, the FAS can be adapted to the desired stiffness curve by offsetting the spring fix point. Specially designed off-axis magnets with 12-bit hall sensors and bidirectional serial synchronous (BiSS) interface measure the tendon force.

TENDON-DRIVEN ELASTIC CONTINUUM NECK JOINT

The tendon actuation system of the fingers from the previous section is also used for the tendon-driven neck. Contrary to the

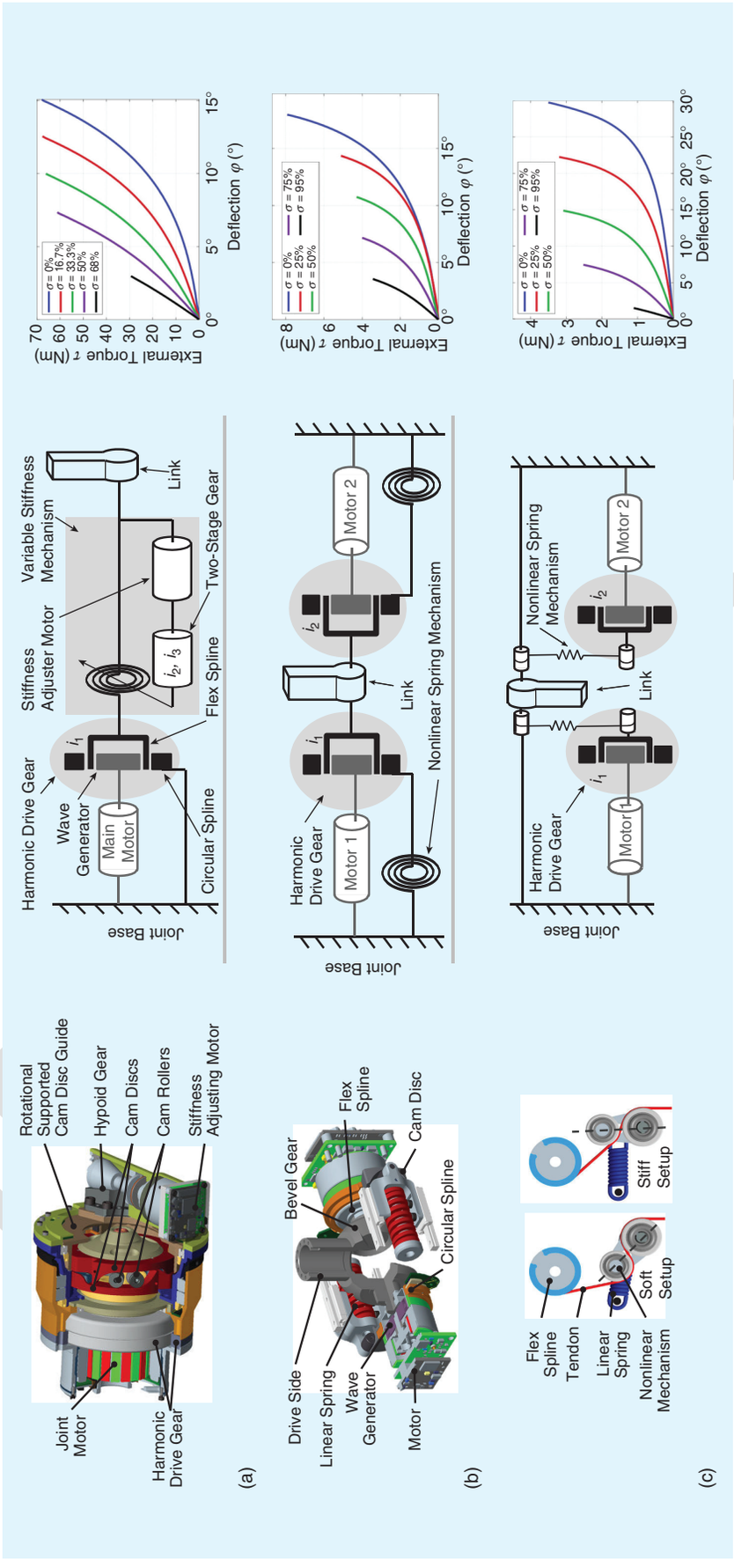

FIGURE 4. (a)–(c) The VSAs of neoDavid: (a) FSJ, (b) BAVS, and (c) FAS. From left to right: CAD models, actuator principles, and external torque versus passive deflection characteristic in five stiffness settings varying from minimum to maximum.

fixed kinematics of the finger joints, the neck is realized by a structurally deformable cylindrical structure molded in silicone [22], which is located between two rigid platforms. The lower platform is mounted toward the shoulders, while the upper platform supports the head and the integrated visual system. To move the head, the four tendons connected to the upper platform are tensioned, applying a load to the silicone structure. By using four tendons not in a straight vertical direction but in two V-shaped kinematics acting similar to a 4 DoF Stewart platform, roll, pitch, and yaw movements of the head are possible. The largest motion is achieved in the look-down configuration, which is primarily required for manipulation.

COMMUNICATION

The present version of the upper body of neoDavid consists of 173 position sensors, three force sensors, and 83 motors. Since neoDavid is a platform for research, the number and type of sensors constantly change. The large number of different motors and sensors poses strong demands on the communication bandwidth [1]. Due to the dynamics of the humanoid robot, a control frequency of 1 kHz was specified for the superimposed robot control. Therefore, the system requires a well-structured, high-bandwidth, and scalable communication architecture. To reserve buffers for additional digital filters, a communication frequency of 3 kHz was defined. The resulting control bandwidth and low latency enable high main control loop frequencies, which are essential to apply control and stability considerations from the continuous time domain. The communication infrastructure was designed hierarchically with SpaceWire as the communication backbone and bidirectional bit pipeline interfaces (BBPIs), a proprietary development (replacing

the originally used BiSS), as the peripheral connection to sensors and actuators.

SpaceWire is a common fieldbus for space applications due to its small footprint and its easy-to-implement features on FPGAs. Additionally, it supports arbitrary topologies (point to point, rings, and trees) and is deterministic for a given topology. Another important aspect is its integrated mechanism for time distribution. Furthermore, with the adapted physical layer presented in [23], high bandwidth and low latency are achieved.

We utilize SpaceWire's integrated time distribution mechanism to synchronize the system's modules, such as the hand, arm, and torso, and to globally align local clocks [24]. To further reduce timing discrepancies, we employ a phase-locked loop (PLL)-based local clock that is synchronized globally, minimizing jitter between spatially separated SpaceWire components. Our SpaceWire setup also enables the recording of all raw data at the main control loop frequency without compromising real-time performance, providing a robust infrastructure for data mining and big data analysis. BBPI follows a similar approach to SpaceWire with respect to (w.r.t.) the possible topologies, synchronization, and the strict hierarchical approach on the peripheral bus level. It has been developed for the data exchange of FPGA-based sensor and actuator modules.

One exception to the described architecture is the COTS mobile platform, which contains a built-in real-time (RT) computer like the other subsystem. Communication with this RT computer, however, is not implemented via SpaceWire but over Ethernet via ROS topics connected to links and nodes. At the current state, Ethernet communication and power supply to neoDavid are tethered.

MOTION AND INTERACTION CONTROL

The quest for high mechanical robustness and dynamic performance motivated the design of robots with VSA joints. However, the incorporation of mechanical compliance introduces underactuation and unwanted oscillatory dynamics, making control a challenging task. This section discusses how we achieve the objective of robust and precise manipulation with neoDavid from a control perspective.

The innovative concept of quasi-full actuation (QFA) was developed to unify the control design and analysis for both rigid and elastic joint robots (EJRs) [25], including neoDavid. This framework can be interpreted as a generalization of [26] and [27], where the equivalence principle is used to achieve gravity compensation and set-point regulation.

The core idea of QFA revolves around a simultaneous transformation of coordinates and inputs on the extended phase space. This transformation enables us to treat EJRs as if they were fully actuated and input/output passive [25]. Through the concept of QFA, we pursue "minimalistic" control designs, where the desired system behavior is obtained by the least feedback modification of its dynamics. This approach is particularly well suited for elastic systems like neoDavid. Our lab experiments have consistently shown that control approaches that significantly modify or override the inherent rigid robot dynamics tend to exhibit unstable behavior when implemented on actual hardware. This problem becomes more pronounced as joint compliance increases, reducing mechanical bandwidth. This observation sparked the development of a series of passivity-based control schemes tailored for robots with elastic or visco-elastic joints, collectively known as *elastic structure preserving (ESP) control* [28]. ESP control adheres to the philosophy of "Do as little as possible, but as much as necessary" and serves as the foundation of our motion and interaction control framework for neoDavid. This framework achieves the following:

- safe and compliant interaction
- uniform asymptotically stable motion tracking in both joint and task spaces
- a passive and robust closed-loop system
- high positioning accuracy.

Our ESP-based control framework empowers EJRs to perform commercially viable tasks, as demonstrated in the "Validation and Discussion" section. Notably, neoDavid's arms achieve a joint positioning accuracy of 72 μrad [29], which is the link sensor resolution. This level is comparable to that of rigid robots. In contrast to conventional impedance control methods [30], [31], where the renderable stiffness is bounded by the stiffness of the elastic element within the SEA, the ESP control concept overcomes this limitation [28]. The passivity of the closed-loop system is guaranteed, irrespective of the impedance control parameters. This highly desirable property is a direct result of the structure-preserving nature of the ESP approach, where the generated closed-loop dynamics consists solely of passive elements: masses, springs, and dampers.

CONTROL APPROACHES

David utilizes various actuation principles, each presenting distinct control challenges; see Figure 4. A common challenge across its compliant actuators is the inherent underactuation,

TABLE 2. The properties of neoDavid's VSAs.

ACTUATOR	WEIGHT	MAX. TORQUE/FORCE	SPRING ENERGY	MAX. DEFLECTION	MOTOR MODULE	GEAR
FSJ	1.4 kg	68 Nm	5.3 J	±15°	ILM50x14	HD CSD-25 80/1
					ILM25x8	HD CSD-8 and hypoid 1000/1
BAVS	0.25 kg, 0.75 kg	8 Nm	0.9 J	±22.5°, ±18°	2x ILM25x4,8	HD CSD-8 100/1
FAS	N/A	120 N	0.1 J	2-7 mm (30°)	2x ILM25x4,8	HD CSD-8 100/1

lack of input/output passivity [32], and highly nonlinear stiffness characteristics.

ASYMMETRIC VSA

Asymmetric VSA elements utilize a primary motor to control the link's equilibrium position, with a secondary motor adjusting stiffness. Examples include the FSJ, as shown in Figure 5, and the torso's vertical axis. Usually, the adjuster dynamics can be neglected during control design as it is comparably slow relative to the dominating dynamics of the main motor. To achieve uniform globally asymptotically stable motion tracking, combined with direct link-side damping injection, we apply the ESP controller from [28].

BI-ANTAGONISTIC VSAS

In contrast to asymmetric VSA, bi-antagonistic setups couple the effects of both motors, requiring the consideration of both motor dynamics in control design, increasing complexity. Depending on the motor's relative motion, either the stiffness or the equilibrium position is altered. In [33], we exploited this property to extend the ESP concept to achieve simultaneous motion tracking and joint stiffness control. The controller is employed on the BAVS actuator in forearm rotation.

TENDON-DRIVEN ACTUATION

Tendon routing introduces a configuration-dependent coupling of elastic torques, requiring the coordinated movement of multiple motors to move a single link. The null space of the finger coupling matrix offers flexibility in varying stiffness behavior. Avoiding slack is addressed by maintaining sufficient and appropriate pretension. For the tendon-actuated torso, we use a cascaded control approach, ensuring the desired tendon pretension with an inner-loop tendon-force controller, while an outer-loop joint impedance controller facilitates motion tracking. Following the aforementioned ESP control philosophy, our controller preserves the coupled elastic structure of the finger, achieving closed-loop dynamics with minimal modifications [34].

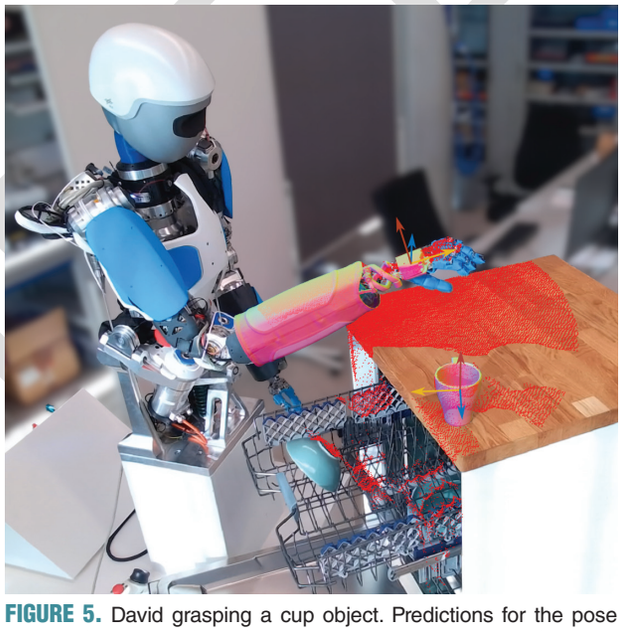

FIGURE 5. David grasping a cup object. Predictions for the pose and configuration of the forearm, wrist, palm, and cup from the M3T tracker are visualized as a pink overlay. Red dots represent depth information point cloud from the sensor. Please note the missing depth information, e.g., on the table surface, by the "shadows" of the arm and the cup.

ELASTIC CONTINUUM NECK

For control purposes, the dynamics of the continuously deformable neck is reduced to a rigid body (head) on a nonlinear spring with 6 DoF. The characteristics of the mapping from generalized spring forces to rigid-body coordinates were obtained through identification [22]. The control loop employs a cascaded approach with inner tendon-force controllers, ensuring desired tendon-force tracking. The outer loop utilizes partial feedback linearization to account for the underactuation and enable the trajectory tracking of chosen outputs, including head orientations and neck compression.

PERCEPTION

To perceive its environment, neoDavid is equipped with an Azure Kinect RGB-D camera mounted on a structurally elastic neck, imposing significant challenges for accurately measuring or estimating the pose of the object or the hand. Pose estimation is crucial for manipulation tasks. In the following, we illustrate how computer vision and proprioception enhance the manipulation skills.

COMPUTER VISION

To estimate the pose of an object and the hand, a 3D object M3T tracker[1] is employed to estimate the poses of objects and the robot hand continuously. It runs at the full camera frequency of 30 Hz. M3T is a highly efficient modular algorithm developed at DLR that supports a wide range of kinematic structures, object characteristics, and camera configurations. In comparison to other tracking approaches, such as [35] or [36], M3T fuses region-based red, green, blue (RGB), depth, and texture information and incorporates data from joint sensors. The applied region-based approach uses color statistics to differentiate between sparse representations of the object silhouette and background, and it estimates the pose that best explains the segmentation. The integrated depth modality uses an Iterative Closest Point Algorithm-like technique that minimizes the distance between model points and depth measurements [37]. To consider connections between rigid bodies in the forearm, wrist, and hand, we accurately model the closed wrist kinematics using joints and constraints within the M3T framework [38]. The initial 6D poses of the manipulated objects are estimated by applying a 2D bounding box detector followed by our augmented autoencoder [39]. An example image that shows the tracking of the hand and a manipulated cup object is shown in Figure 5.

[1]M3T: **M**ulti-body, **M**ulti-modality, and **M**ulti-camera 3D object Tracking; see https://github.com/DLR-RM/3DObjectTracking for more details

PROPRIOCEPTION

Proprioception allows neoDavid to cope with the challenge that objects might get lost in tracking due to fast motions and large occlusions. The underlying reason for this is the design of the tracker to locally optimize in a given image and estimate minor pose changes from consecutive frames. Therefore, to improve the pose estimation for the right arm, M3T incorporates the forward kinematics and joint measurements into the optimization process. In the case of strong pose estimation deviations above a certain threshold, the tracking optimization is constrained to the forward kinematics [38]. Consequently, this helps to avoid tracking loss, improves robustness, and thus positively affects the accuracy of the tracker. In summary, one can conclude that, similar to humans, this allows neoDavid to have a degree of proprioception in the sense of combining the approximate hand position with visual feedback for precise estimations.

MANIPULATION

The initial step in the planning process for a desired manipulation task is an analysis of the workspace. By identifying potential improvements to the task execution location, this allows for a more effective planning of the manipulation task. Once the *offline task planning* is done, our *motion planner* is used for the efficient computation of collision-free and smooth trajectories. To *grasp the objects*, the motion planner computes a trajectory to move the hand of the robot in the vicinity of the object's location. From this proximity, the planner generates a local approach motion of the palm w.r.t. the object pose. Subsequently, the fingers move toward the object and finally close to grasp and manipulate the object.

OFFLINE TASK PLANNING WITH CAPABILITY MAPS

The workspace analysis done before the task uses the capability maps [40], which provide a visualization of the reachable workspace of the robot and a color-coded percentage of possible hand orientations per reachable discrete point, called the *capability index*. Thanks to the color-coded representation of the capabilities, we can also use this tool to observe the impact on the workspace reachability of an extension of the kinematic chain of the robot. As illustrated in Figure 6(a), the incorporation of torso joints into the system has resulted in a notable expansion in the size of the capability maps. Another observable change is that the increase in the percentage of possible orientations can be observed as a direct consequence of the extension of the kinematic chain of the robot.

Before the manipulation starts, the reachable workspace is analyzed by means of the capability maps of the robot so that the user can choose a region for the execution of the task, where the manipulation is not only feasible but also as dexterous as possible. The visual information given by the capability maps is complemented by adding the robot and environment to the visualizer scene, as shown in Figure 6(b). As a result, one can observe the expected dexterity represented by the *capability index* in specific areas of the environment and optimize the location for the task setup.

MOTION PLANNING

To exploit the increased reachability of the workspace visible in Figure 6(a), we employ the robotic motion planning library

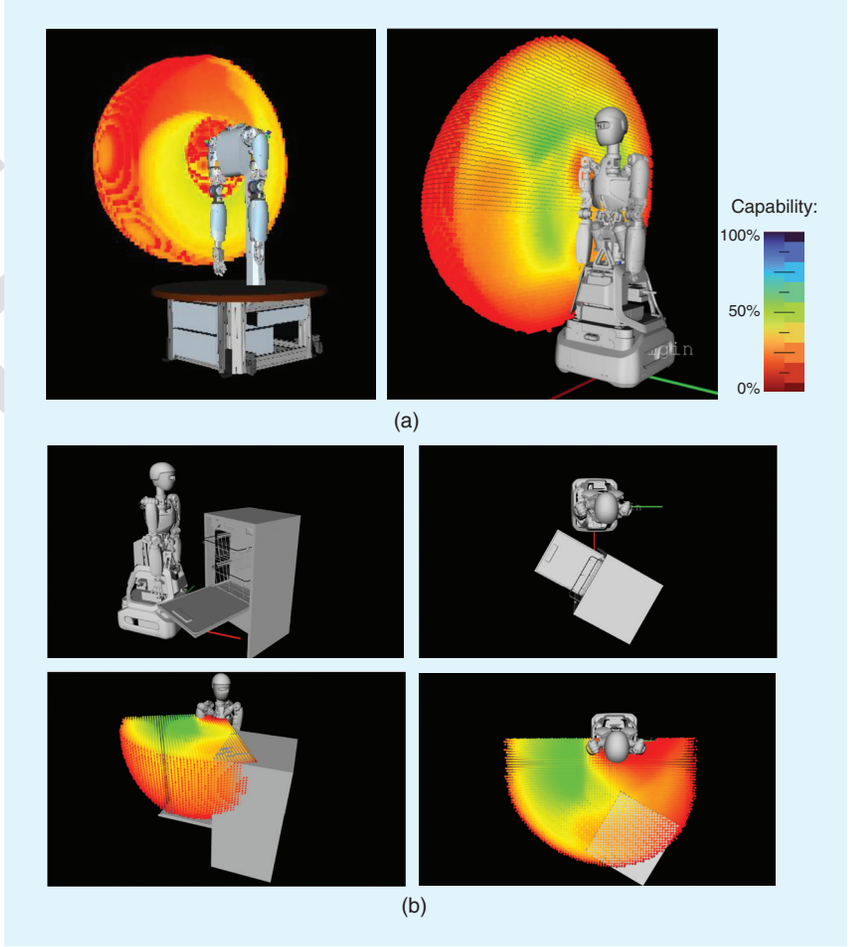

FIGURE 6. The capability maps as a planning tool. In (a), the capabilities of the 7 DoF right arm of David (on the left) are shown in comparison to the 7 + 3 DoF after the addition of the torso (on the right). Further right, the color map shows the *capability index* represented. In (b), the maps provide information on the dexterity of interactions with the scene (bottom), allowing us to plan the task setup using a visualization of the robot with the task environment (top). (a) Reachability and capability before and after the addition of the torso. (b) Offline planning of task setup using capability maps.

[41]. It is able to efficiently handle the extended joint space of the right arm with the torso and provide smooth and collision-free trajectories toward Cartesian or joint space targets. Through a flexible Python interface, we are able to add objects to the motion planning environment and consider them inside the motion plan. A visual interface, shown in Figure 7, displays the information considered by the motion planner as well as the path executed by the planned motion. Additionally, the flexibility of the motion planner allows one to momentarily ignore desired collisions (e.g., for interactions with the task objects) and to add/remove objects from the environment during task execution. To approach the objects, the motion planner first plans a Cartesian path for the palm to an object-fixed Cartesian target in close vicinity to the object's location. Meanwhile, the corresponding arm trajectories in joint space are computed. The approaching motion is executed via the introduced controller (see the "Control Approaches" section) as the first step. As the second step, the finger grasping motion is executed, which will be further illustrated in the following section.

OBJECT GRASPING AND IN-HAND MANIPULATION

Thanks to its anthropomorphic multifingered hand design, the DLR robot neoDavid is kinematically capable of performing object grasping as well as in-hand manipulation tasks. Nevertheless, enabling it to either grasp or manipulate an object involves varying levels of complexity of motion planning and control.

GRASPING

In this section, we refer to *grasping* as the process of immobilizing objects by generating and executing finger motion, once the palm has been positioned in close proximity to the object. The final finger locations are predesigned based on the object's shape and pose and the finger's geometry. To ensure a stable grasp (e.g., satisfying the force-closure condition [42, Definition 4], a heuristic offset is added to the desired configuration to implicitly apply sufficient internal force. The trajectory of each finger joint is generated with a third-order polynomial interpolation w.r.t. time with the upper-bounded velocity and acceleration. The trajectories are executed by impedance control, as described in cf. the "Tendon-Driven Actuation" section. However, in practice, grasp execution failures often occur due to sensing inaccuracies and the presence of friction as well as the fact that the motion is executed in an open-loop manner. To address these issues and enable more dexterous manipulation, e.g., rotating a wooden pentagonal toy (see the supplementary video available at https://doi.org/10.1109/MRA.2025.3599706) in the "Fine Manipulation of Tools and Objects" section, the real-time feedback of the object pose and finger-object contact locations are required.

OBJECT IN-HAND LOCALIZATION

A fundamental task in object localization is to robustly and continuously estimate reliable finger contact point locations by fusing data from various proprioceptive sensors. In our work [43], we employed an extended Kalman filter (EKF) that integrates the finger joint position and torque measurement as well as the object pose prediction from the tracker to estimate the contact point locations during the grasping. Additionally, when the object is partially or completely occluded by the hand, the EKF computes a correction term to enhance the accuracy of the tracker's object pose estimation.

IN-HAND MANIPULATION

Using the estimated object state, the developed object-impedance controller [44] is designed to achieve compliant object repositioning within the hand while ensuring that the object remains securely held. The motion control comprises two components: 1) object wrench generation, which leads to changes in the object's pose, and 2) internal wrench generation, which accounts for changes in the object's internal forces. Since contact forces exerted by the fingers are unilateral, the final wrench distribution for each fingertip is formulated as a real-time feasible convex quadratic programming problem [45] that satisfies the friction cone condition [46, eq. (5.3)]. The desired finger wrenches are then mapped to reference joint torques, which are passed to the inner-loop tendon-force controller.

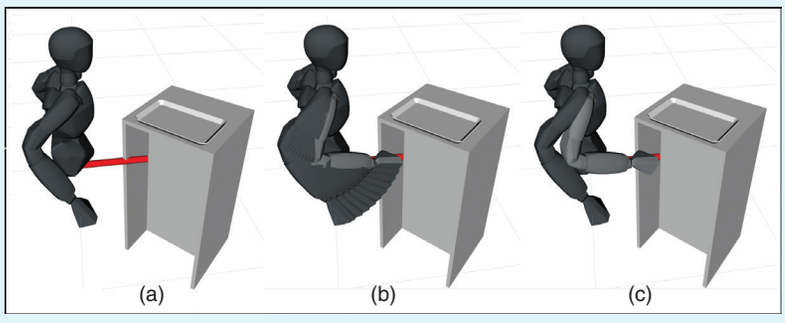

FIGURE 7. The visual interface from the motion planner shows, in (a), the 3D collision model along with the elements of the environment. In (b), the path computed toward a given goal can be checked. In (c), the target configuration is highlighted in light grey.

VALIDATION AND DISCUSSION

Since a universal humanoid robot is, by definition, designed to perform a wide variety of different tasks, it is challenging to validate its versatility just by a few measurable use cases. Therefore, the versatile character of the robot in terms of dexterity and robustness is validated in exemplary experimental applications with fundamentally different objectives, e.g., handling a drill hammer, fine manipulation of a pipette, and emptying a dishwasher. These applications are selected as challenging service robotics tasks in the context of craftsmanship, industry, and household. The

accompanying video (available at https://doi.org/10.1109/MRA.2025.3599706) illustrates specific instances of applications that exemplify the objectives discussed. In the following, our results are grouped according to their main contribution to the objectives of the "Objectives" section.

HUMAN APPEARANCE

With the upper body of neoDavid, we achieved a human-like appearance with similar shape and motion axes located in a similar area as the human, e.g., three intersecting axes in the abdomen, shoulder, and wrist. Also, the 55-kg upper body, including the torso and head, is similar to a human. The right forearm is bulkier and heavier (4.6 kg) than that of an average human, which is caused by the 44 motor modules driving the right hand and wrist. In this part, we chose superhuman motion capabilities over strict human appearance. A human has 19 main muscles for hand actuation in the forearm, where we have 38 motor modules instead to be able to move all 20 DoF of the hand individually. The neoDavid system has no legs but a heavy four-wheeled base for a stable stance. This decision was due to the fact that we want to focus on manipulation tasks in applications where a small footprint is not absolutely necessary. When we expanded the system to include mobility, leg-based systems and control did not seem mature enough to provide stable and reliable support for an upper body performing fine manipulation with high external forces. Furthermore, the commercial availability of four-wheeled platforms made it easy and cost-effective to integrate mobility.

MODULARITY IN THE SYSTEM ARCHITECTURE

The modularization in neoDavid is realized in several hierarchical levels. First, all body segments (see Figure 8(a)) can be switched on/off and controlled separately, and they can be mechanically separated easily in case of maintenance. This makes debugging and failure handling dramatically simpler. Second, for its 52 DoF and 91 motors, only six different motor modules and five types of communication electronics are used; see Figure 8(b). The left and right arms can be transformed vice versa by a simple remount; only a few housing parts and the wrist are different. Despite the many modules in our real-time communication, the jitter between spatially separated SpaceWire components within each 3-kHz control loop of the system is ±16 ns, which is achieved by introducing a globally synchronized PLL-based local clock [24].

ROBUSTNESS AGAINST IMPACTS

Mechanical robustness against impacts during operation is one of the main motivations for the development of neoDavid. Consequently, we have conducted experimental validations

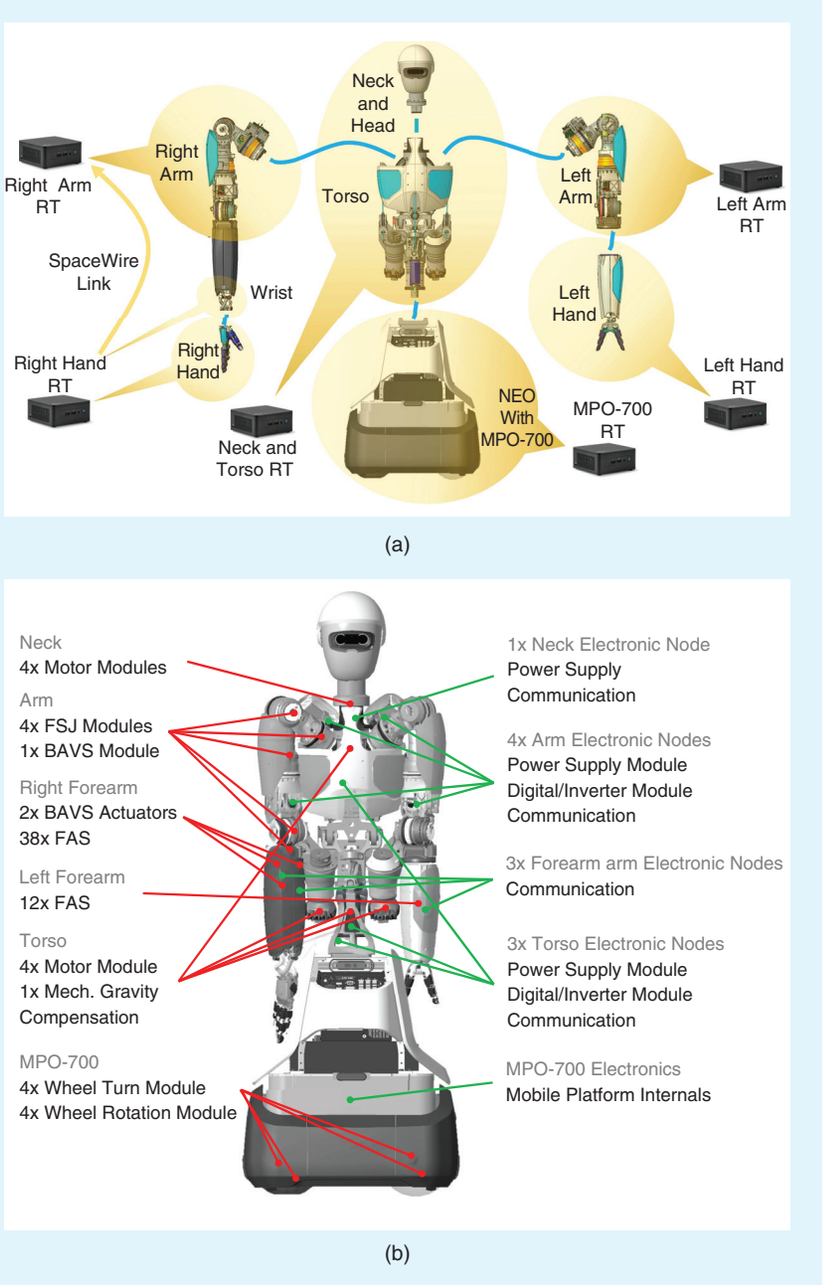

FIGURE 8. (a) The subsystems of neoDavid and their real-time computer nodes and distribution. Information from the right wrist is transmitted directly via SpaceWire to the right arm computer to provide 7 DoF arm control without time delay. (b) The actuators (red) and electronic nodes (green) of neoDavid.

already in the early stages of development, shown in the supplementary video available at https://doi.org/10.1109/MRA.2025.3599706. The fingers withstood impacts of an 840-g hammer with an impact velocity of approximately 2 m/s without any damage [21]. Also, no harm was done to the arm when we hit it with a baseball bat and transferred 22 J of impact energy [16]. Robustness of the arm, including control, was validated in [28] with a 3-kg mass swinging against the forearm with an impact energy of 7.7 J. The same swinging mass was used to hit the head with an impact energy of 6.2 J, demonstrating the robustness of the structurally elastic neck. The overload protection feature of the face shield is also visible. The visor is attached to the head by magnets to absorb the impact energy. All covers and the neck structure remain intact after impact.

FAST AND POWERFUL INTERACTION WITH TOOLS

Dynamic forces in combination with high static forces on the grip handle are typical for the use of power tools. Drilling holes into a pavement slab made of concrete addresses several challenges of craftsmanship tasks with power tools. The guiding hand and arm have to withstand external forces while performing a coordinated movement and the operation of the tool. In the experiment, we used a 2.0-kg Bosch Uneo Maxx drill hammer with a single hit force rating (European Power Tool Association) of 0.6 J and drilled more than 100 holes in 5-cm concrete slabs with full machine power (see the supplementary video available at https://doi.org/10.1109/MRA.2025.3599706).

Surprisingly high peak forces are also required during everyday applications in household scenarios. The torque/force $\boldsymbol{\tau}_{p,\max}$, $\mathbf{F}_{p,\max}$ analysis of opening the door in the dishwasher application is given in Figure 9 (see the supplementary video available at https://doi.org/10.1109/MRA.2025.3599706). Peak velocity is key to dynamic applications such as throwing a ball, which was thrown more than 5.1 m with a Dynamic Motion Primitives generated trajectory and caught by the robot Justin (see the supplementary video available at https://doi.org/10.1109/MRA.2025.3599706).

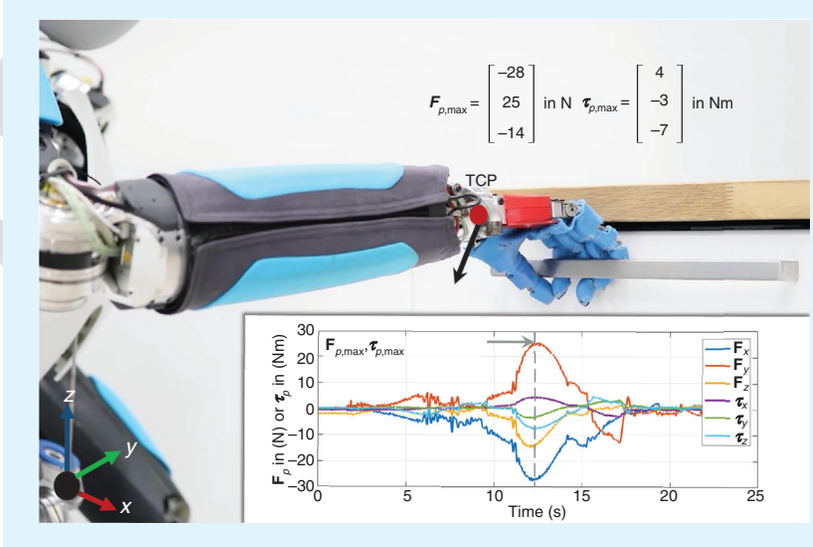

FIGURE 9. Opening the dishwasher: time evolution and maximal values of the pulling torque/force $\boldsymbol{\tau}_{p,\max}$, $\mathbf{F}_{p,\max}$, required to unlock the sealing of the door, expressed in the tool center point frame, which is located in the middle of the wrist.

FINE MANIPULATION OF TOOLS AND OBJECTS

We demonstrate our in-hand manipulation framework from the "Object Grasping and In-Hand Manipulation" section by reorienting objects of different shapes between three and five fingers (see the supplementary video available at https://doi.org/10.1109/MRA.2025.3599706). This basic skill is essential for manipulation tasks. Figure 10(b) and (c) shows the results of the in-hand reorientation of the pentagon-shaped object depicted in Figure 10(a). A periodic triangular reference is applied that results in a continuous motion of the object [44]. Furthermore, the position and orientation tracking deviations of two additional objects were quantitatively assessed, as detailed in [44], Table 1.

Using a pipette mainly involves perception and fine manipulation skills (see the supplementary video available at https://doi.org/10.1109/MRA.2025.3599706). The trigger of the pipette is pressed with the thumb to use the tool while maintaining a stable grip with the fingers. This sequence of grasp transitions and in-hand manipulation was possible only due to the high number of DoFs and the range of motion, especially in the carpometacarpal joint of the thumb.

Same as for the pipette, the drill hammer was held during operation with four fingers in a power grasp, and the trigger was operated by the remaining finger, which was, in this case, the index finger (see the supplementary video available at https://doi.org/10.1109/MRA.2025.3599706). Also, with this power tool, separately movable fingers are the key factor for successful operation, which indicates that multiple active DoFs are necessary for many tools, in particular, power tools.

Emptying a dishwasher is a demanding task from a robotics perspective. Various consecutive subtasks need to be completed successfully in a row to accomplish the whole chore. We analyzed the spatial workspace and the dishwasher setup with capability maps to place the dishwasher in an area where neoDavid can open its door and trays, and it can reach all objects as well as the area on top of the dishwasher to place the objects; see also Figure 6. A significant aspect of the process of emptying a dishwasher is the act of grasping the various items contained within. We show the overall grasp success of one of

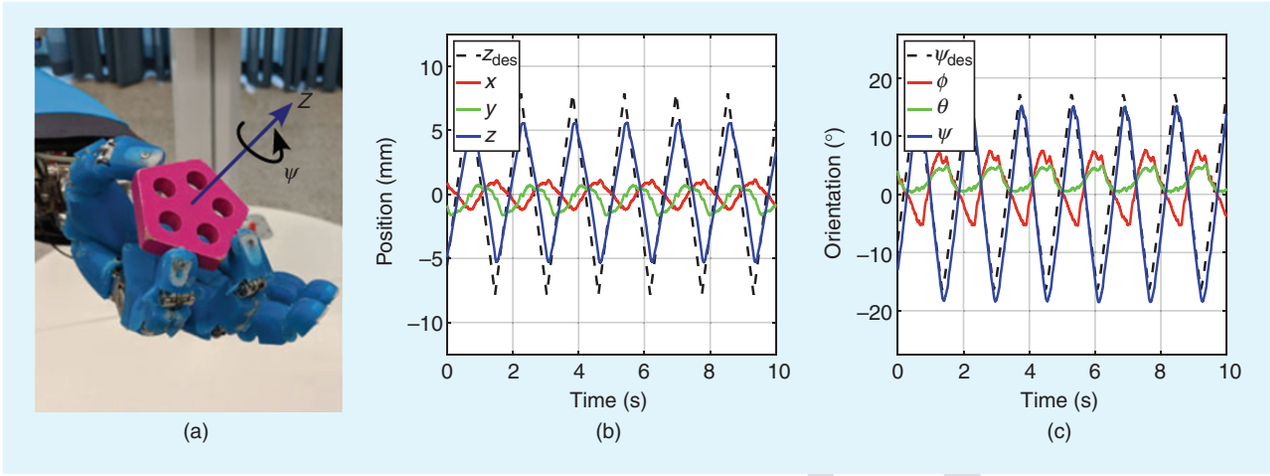

FIGURE 10. (a) An illustration of the handled object. (b) and (c): Cartesian accuracy in terms of translation and orientation, while a desired motion is applied in specific directions.

the objects from the dishwasher in Figure 11. As introduced previously in the "Manipulation" section, in our implementation, the vision system provides a Cartesian target for the planner to approach the object and finally grasp it. The Cartesian target is given as a predefined reference of the palm pose w.r.t. the object frame to grasp. This approach produces a repeatable behavior, achieving a grasp success rate of 73.75% on the highlighted positions of the rack. In the plot, it can be observed how the first position of the rack is declared as unfeasible since the object does not fit in. However, in the adjoining positions, the object fits in the rack, and the robot has a high grasp success rate until the final slots of the rack. At the rearward positions in the rack, the grasp starts to fail given a decrease in the kinematic reachability of the system, which hinders the predefined palm pose w.r.t. the object to be successfully reached, therefore resulting in a failure to grasp. Visibly, the success rate of this method relies highly on both finding the palm pose w.r.t. the object that enables the grasp but also on the kinematics able to reach the predefined pose.

CONCLUSION AND FUTURE WORK

neoDavid's synergistic integration of embodiment (hardware) and computation (software) is the key enabling factor for its robust and dexterous manipulation capabilities [47]. The robot's physically compliant actuation technology spans its entire body, with each actuator providing exceptional shock resistance and enabling highly dynamic motions. In parallel, advanced control algorithms enable cobot-level accuracy, facilitating fine and dexterous manipulation, with their passive-induced robustness complementing the mechanical resilience of the hardware. Research advancements in mechatronics, control, capability mapping, perception, and manipulation have elevated the system's capabilities to a level where it is ready to execute complex tasks. All developments have been tested and verified through diverse experiments.

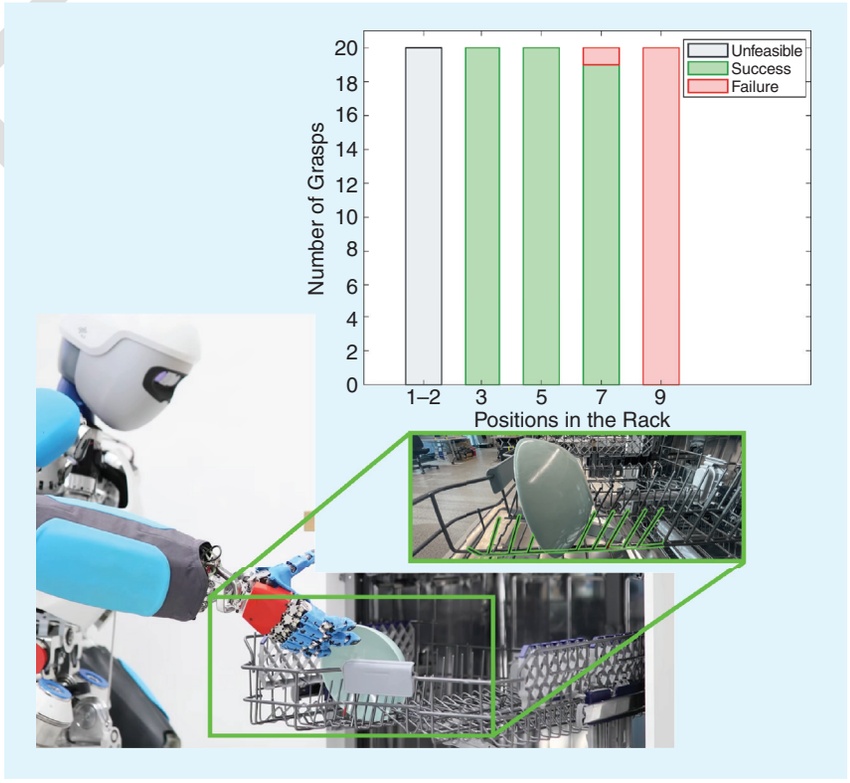

FIGURE 11. The grasp success of a bowl from the dishwasher. The predefined reference pose shows a repeatable behavior in a limited number of rack positions. The back positions of the rack present failures due to reduced kinematic reachability of these targets. The first positions on the rack are tagged as unfeasible due to the lack of space to set the object.

Our future work will focus on developing a more streamlined computer architecture with fewer real-time computers. This approach promises to achieve higher performance in whole-body control by reducing time delays due to current Ethernet communication. Additionally, it will consume less power and have a smaller build volume. These improvements will also enable untethered operation for unrestricted navigation.

ACKNOWLEDGMENT

This article has supplementary downloadable material available at https://doi.org/10.1109/MRA.2025.3599706, provided by the authors.

AUTHORS

Sebastian Wolf, German Aerospace Center, Institute of Robotics and Mechatronics, D-82234 Wessling, Germany. E-mail: Sebastian.Wolf@dlr.de.

Thomas Bahls, German Aerospace Center, Institute of Robotics and Mechatronics, D-82234 Wessling, Germany. E-mail: Thomas.Bahls@dlr.de.

Bastian Deutschmann, German Aerospace Center, Institute of Robotics and Mechatronics, D-82234 Wessling, Germany. E-mail: Bastian.Deutschmann@dlr.de.

Alexander Dietrich, German Aerospace Center, Institute of Robotics and Mechatronics, D-82234 Wessling, Germany. E-mail: Alexander.Dietrich@dlr.de.

Marie Harder, ifp consulting GmbH & Co. KG, D-85748 Garching, Germany. E-mail: marie.harder@ifpconsulting.de.

Hannes Höppner, Berliner Hochschule für Technik, Humanoide Robotik, 13353 Berlin, Germany. E-mail: Hannes.Hoeppner@bht-berlin.de.

Cynthia Hofmann, German Aerospace Center, Institute of Robotics and Mechatronics, D-82234 Wessling, Germany. E-mail: Cynthia.Hofmann@dlr.de.

Ana Huezo Martin, German Aerospace Center, Institute of Robotics and Mechatronics, D-82234 Wessling, Germany. E-mail: Ana.HuezoMartin@dlr.de.

Leonard Klüpfel, German Aerospace Center, Institute of Robotics and Mechatronics, D-82234 Wessling, Germany. E-mail: Leonard.Kluepfel@dlr.de.

Henry Maurenbrecher, German Aerospace Center, Institute of Robotics and Mechatronics, D-82234 Wessling, Germany. E-mail: Henry.Maurenbrecher@dlr.de.

Xuming Meng, Agile Robots SE, D-81369 Munich, Germany. E-mail: xuming.meng@agile-robots.com.

Manuel Keppler, German Aerospace Center, Institute of Robotics and Mechatronics, D-82234 Wessling, Germany. E-mail: Manuel.Keppler@dlr.de.

Anne E. Reichert, German Aerospace Center, Institute of Robotics and Mechatronics, D-82234 Wessling, Germany. E-mail: Anne.Reichert@dlr.de.

Manuel Stoiber, Stoiber GmbH Maschinenbau, A-4122 Arnreit, Austria. E-mail: manuel.stoiber@stoiber.eu.

Markus Bihler, KINETIK Space GmbH, D-82205 Gilching, Germany. E-mail: bihler@kinetik.space.

Maxime Chalon, KINETIK Space GmbH, D-82205 Gilching, Germany. E-mail: chalon@kinetik.space.

Oliver Eiberger, German Aerospace Center, Institute of Robotics and Mechatronics, D-82234 Wessling, Germany. E-mail: Oliver.Eiberger@dlr.de.

Werner Friedl, German Aerospace Center, Institute of Robotics and Mechatronics, D-82234 Wessling, Germany. E-mail: Werner.Friedl@dlr.de.

Markus Grebenstein, German Aerospace Center, Institute of Robotics and Mechatronics, D-82234 Wessling, Germany. E-mail: Markus.Grebenstein@dlr.de.

Maged Iskandar, German Aerospace Center, Institute of Robotics and Mechatronics, D-82234 Wessling, Germany. E-mail: Maged.Iskandar@dlr.de.

Viktor Langofer, German Aerospace Center, Institute of Robotics and Mechatronics, D-82234 Wessling, Germany. E-mail: Viktor.Langofer@dlr.de.

Martin Pfanne, Agile Robots SE, D-81369 Munich, Germany. E-mail: martin.pfanne@agile-robots.com.

Antonin Raffin, German Aerospace Center, Institute of Robotics and Mechatronics, D-82234 Wessling, Germany. E-mail: Antonin.Raffin@dlr.de.

Jens Reinecke, German Aerospace Center, Institute of Robotics and Mechatronics, D-82234 Wessling, Germany. E-mail: Jens.Reinecke@dlr.de.

Tilo Wüsthoff, German Aerospace Center, Institute of Robotics and Mechatronics, D-82234 Wessling, Germany. E-mail: Tilo.Wuesthoff@dlr.de.

Alin Albu-Schäffer, German Aerospace Center, Institute of Robotics and Mechatronics, D-82234 Wessling, Germany. E-mail: Alin.Albu-Schaeffer@dlr.de.

REFERENCES

[1] M. Grebenstein et al., "The DLR hand arm system," in *Proc. IEEE Int. Conf. Robot. Automat.*, 2011, pp. 3175–3182, doi: 10.1109/ICRA.2011.5980371.

[2] M. Grebenstein, M. Chalon, G. Hirzinger, and R. Siegwart, "Antagonistically driven finger design for the anthropomorphic DLR hand arm system," in *Proc. 10th IEEE-RAS Int. Conf. Humanoid Robots*, Piscataway, NJ, USA: IEEE Press, 2010, pp. 609–616, doi: 10.1109/ICHR.2010.5686342.

[3] C. Borst et al., "Rollin' Justin - Mobile platform with variable base," in *Proc. IEEE Int. Conf. Robot. Automat.*, 2009, pp. 1597–1598, doi: 10.1109/ROBOT.2009.5152586.

[4] N. G. Tsagarakis, S. Morfey, G. Medrano Cerda, L. Zhibin, and D. G. Caldwell, "COMpliant huMANoid COMAN: Optimal joint stiffness tuning for modal frequency control," in *Proc. IEEE Int. Conf. Robot. Automat.*, 2013, pp. 673–678, doi: 10.1109/ICRA.2013.6630645.

[5] A. Ajoudani et al., "A manipulation framework for compliant humanoid COMAN: Application to a valve turning task," in *Proc. IEEE-RAS Int. Conf. Humanoid Robots*, 2014, pp. 664–670, doi: 10.1109/HUMANOIDS.2014.7041434.

[6] N. G. Tsagarakis et al., "WALK-MAN: A high-performance humanoid platform for realistic environments," *J. Field Robot.*, vol. 34, no. 7, pp. 1225–1259, 2017, doi: 10.1002/rob.21702. [Online]. Available: https://onlinelibrary.wiley.com/doi/abs/10.1002/rob.21702

[7] F. Negrello et al., "Humanoids at work: The WALK-MAN robot in a post-earthquake scenario," *IEEE Robot. Autom. Mag.*, vol. 25, no. 3, pp. 8–22, Sep. 2018, doi: 10.1109/MRA.2017.2788801.

[8] M. G. Catalano, G. Grioli, E. Farnioli, A. Serio, C. Piazza, and A. Bicchi, "Adaptive synergies for the design and control of the Pisa/IIT SoftHand," *Int. J. Robot. Res.*, vol. 33, no. 5, pp. 768–782, 2014, doi: 10.1177/0278364913518998.

[9] G. Lentini et al., "Alter-Ego: A mobile robot with a functionally anthropomorphic upper body designed for physical interaction," *IEEE Robot. Autom. Mag.*, vol. 26, no. 4, pp. 94–107, Dec. 2019, doi: 10.1109/MRA.2019.2943846.

[10] H. Song, Y.-S. Kim, J. Yoon, S.-H. Yun, J. Seo, and Y.-J. Kim, "Development of low-inertia high-stiffness manipulator LIMS2 for high-speed manipulation of

foldable objects," in *Proc. IEEE/RSJ Int. Conf. Intell. Robots Syst. (IROS)*, 2018, pp. 4145–4151, doi: 10.1109/IROS.2018.8594005.

[11] K. Kawaharazuka et al., "Component modularized design of musculoskeletal humanoid platform Musashi to investigate learning control systems," in *Proc. IEEE/RSJ Int. Conf. Intell. Robots Syst. (IROS)*, 2019, pp. 7300–7307, doi: 10.1109/IROS40897.2019.8968068.

[12] B. Vanderborght et al., "Variable impedance actuators: A review," *Robot. Auton. Syst.*, vol. 61, no. 12, pp. 1601–1614, 2013, doi: 10.1016/j.robot.2013.06.009. [Online]. Available: Http://www.sciencedirect.com/science/article/pii/S0921889013001188

[13] O. M. Andrychowicz et al., "Learning dexterous in-hand manipulation," *Int. J. Robot. Res.*, vol. 39, no. 1, pp. 3–20, 2020, doi: 10.1177/0278364919887447.

[14] F. Lotti, P. Tiezzi, G. Vassura, L. Biagiotti, G. Palli, and C. Melchiorri, "Development of UB hand 3: Early results," in *Proc. IEEE Int. Conf. Robot. Autom.*, 2005, pp. 4488–4493, doi: 10.1109/ROBOT.2005.1570811

[15] R. Ozawa, K. Hashirii, Y. Yoshimura, M. Moriya, and H. Kobayashi, "Design and control of a three-fingered tendon-driven robotic hand with active and passive tendons," *Auton. Robots*, vol. 36, nos. 1–2, pp. 67–78, 2014, doi: 10.1007/s10514-013-9362-z.

[16] S. Wolf, O. Eiberger, and G. Hirzinger, "The DLR FSJ: Energy based design of variable stiffness joints," in *Proc. IEEE Int. Conf. Robot. Automat.*, Shanghai, China, 2011, pp. 5082–5089, doi: 10.1109/ICRA.2011.5980303.

[17] W. Friedl, M. Chalon, J. Reinecke, and M. Grebenstein, "FRCEF: The new friction reduced and coupling enhanced finger for the Awiwi hand," in *Proc. IEEE-RAS 15th Int. Conf. Humanoid Robots (Humanoids)*, 2015, pp. 140–147, doi: 10.1109/HUMANOIDS.2015.7363527.

[18] M. Iskandar and S. Wolf, "Dynamic friction model with thermal and load dependency: Modeling, compensation, and external force estimation," in *Proc. IEEE Int. Conf. Robot. Automat. (ICRA)*, Piscataway, NJ, USA: IEEE Press, 2019, pp. 7367–7373, doi: 10.1109/ICRA.2019.8794406.

[19] W. Friedl, H. Höppner, F. Petit, and G. Hirzinger, "Wrist and forearm rotation of the DLR Hand Arm System: Mechanical design, shape analysis and experimental validation," in *Proc. IEEE/RSJ Int. Conf. Intell. Robots Syst.*, Sep. 2011, pp. 1836–1842, doi: 10.1109/IROS.2011.6094616.

[20] J. Reinecke, B. Deutschmann, A. Dietrich, and M. Hutter, "An anthropomorphic robust robotic torso for ventral/dorsal and lateral motion with weight compensation," *IEEE Robot. Autom. Lett.*, vol. 5, no. 3, pp. 3876–3883, Jul. 2020, doi: 10.1109/LRA.2020.2983386.

[21] W. Friedl, M. Chalon, J. Reinecke, and M. Grebenstein, "FAS A flexible antagonistic spring element for a high performance over actuated hand," in *Proc. IEEE/RSJ Int. Conf. Intell. Robots Syst.*, Sep. 2011, pp. 1366–1372, doi: 10.1109/IROS.2011.6094569.

[22] B. Deutschmann, A. Dietrich, and C. Ott, "Position control of an underactuated continuum mechanism using a reduced nonlinear model," in *Proc. 56th Annu. Conf. Decis. Control*, Piscataway, NJ, USA: IEEE Press, 2017, pp. 5223–5230, doi: 10.1109/CDC.2017.8264433.

[23] M. Nickl, S. Jörg, T. Bahls, and M. C. Barry, "Towards high-speed SpaceWire links," in *Proc. 5th Int. SpaceWire Conf.*, 2013, pp. 263–266.

[24] T. Bahls and M. Bihler, "Using SpaceWire time-codes for global synchronization of PLL-based local clocks," in *Proc. 8th Int. SpaceWire Conf.*, Piscataway, NJ, USA: IEEE Press, 2018, pp. 109–112.

[25] M. Keppler, D. Lakatos, C. Ott, and A. Albu-Schäffer, "From underactuation to quasi-full actuation: Aiming at a unifying control framework for articulated soft robots," *Int. J. Robust Nonlinear Control*, vol. 32, no. 9, 2022, doi: 10.1002/rnc.6102.

[26] A. De Luca and F. Flacco, "Dynamic gravity cancellation in robots with flexible transmissions," in *Proc. 49th IEEE Conf. Decis. Control (CDC)*, Piscataway, NJ, USA: IEEE Press, 2010, pp. 288–295, doi: 10.1109/CDC.2010.5718020.

[27] A. De Luca and F. Flacco, "A PD-type regulator with exact gravity cancellation for robots with flexible joints," in *Proc. IEEE Int. Conf. Robot. Autom.*, Piscataway, NJ, USA: IEEE Press, 2011, pp. 317–323, doi: 10.1109/ICRA.2011.5979615.

[28] M. Keppler, D. Lakatos, C. Ott, and A. Albu-Schäffer, "Elastic structure preserving (ESP) control for compliantly actuated robots," *IEEE Trans. Robot.*, vol. 34, no. 2, pp. 317–335, Apr. 2018, doi: 10.1109/TRO.2017.2776314.

[29] M. Keppler, C. Raschel, D. Wandinger, A. Stemmer, and C. Ott, "Robust stabilization of elastic joint robots by ESP and PID control: Theory and experiments," *IEEE Robot. Autom. Lett.*, vol. 7, no. 3, pp. 8283–8290, Jul. 2022, doi: 10.1109/LRA.2022.3187277.

[30] H. Vallery, J. Veneman, E. Van Asseldonk, R. Ekkelenkamp, M. Buss, and H. van Der Kooij, "Compliant actuation of rehabilitation robots," *IEEE Robot. Autom. Mag.*, vol. 15, no. 3, pp. 60–69, Sep. 2008, doi: 10.1109/MRA.2008.927689.

[31] N. L. Tagliamonte and D. Accoto, "Passivity constraints for the impedance control of series elastic actuators," *Proc. Inst. Mech. Eng., Part I: J. Syst. Control Eng.*, vol. 228, no. 3, pp. 138–153, 2014.

[32] M. W. Spong, "Control of flexible joint robots: A survey," Coordinated Sci. Lab., Urbana, IL, USA, Rep. no. UILU-ENG-90-2203, DC-116, Feb. 1990.

[33] M. Harder, M. Keppler, X. Meng, C. Ott, H. Höppner, and A. Dietrich, "Simultaneous motion tracking and joint stiffness control of bidirectional antagonistic variable-stiffness actuators," *IEEE Robot. Autom. Lett.*, vol. 7, no. 3, pp. 6614–6621, Jul. 2022, doi: 10.1109/LRA.2022.3176094.

[34] G. J. Pollayil, X. Meng, M. Keppler, M. Pfanne, A. Bicchi, and C. Ott, "Elastic structure preserving impedance control for nonlinearly coupled tendon-driven systems," *IEEE Control Syst. Lett.*, vol. 6, pp. 1982–1987, 2021, doi: 10.1109/LCSYS.2021.3136749.

[35] T. Schmidt, R. A. Newcombe, and D. Fox, "DART: Dense articulated real-time tracking with consumer depth cameras," *Auton. Robots*, vol. 39, no. 3, pp. 239–258, 2015, doi: 10.1007/s10514-015-9462-z. [Online]. Available: https://api.semanticscholar.org/CorpusID:33254112

[36] V. A. Prisacariu and I. D. Reid, "PWP3D: Real-time segmentation and tracking of 3D objects," *Int. J. Comput. Vis.*, vol. 98, no. 3, pp. 335–354, 2012, doi: 10.1007/s11263-011-0514-3. [Online]. Available: https://api.semanticscholar.org/CorpusID:25321783

[37] M. Stoiber, M. Sundermeyer, and R. Triebel, "Iterative corresponding geometry: Fusing region and depth for highly efficient 3D tracking of textureless objects," in *Proc. IEEE/CVF Conf. Comput. Vis. Pattern Recognit.*, 2022, pp. 6855–6865, doi: 10.1109/CVPR52688.2022.00673.

[38] M. Stoiber, M. Sundermeyer, W. Boerdijk, and R. Triebel, "A multi-body tracking framework - From rigid objects to kinematic structures," 2023, *arXiv:2208.01502*.

[39] M. Sundermeyer, Z.-C. Marton, M. Durner, M. Brucker, and R. Triebel, "Implicit 3D orientation learning for 6D object detection from RGB images," in *Proc. Eur. Conf. Comput. Vis. (ECCV)*, 2018, pp. 712–729.

[40] O. Porges, T. Stouraitis, C. Borst, and M. A. Roa, "Reachability and capability analysis for manipulation tasks," in *Proc. 1st Iberian Robot. Conf. (ROBOT)*, Cham, Switzerland: Springer-Verlag, 2014, pp. 703–718.

[41] P. Lehner and A. Albu-Schäffer, "The repetition roadmap for repetitive constrained motion planning," *IEEE Robot. Autom. Lett.*, vol. 3, no. 4, pp. 3884–3891, Oct. 2018, doi: 10.1109/LRA.2018.2856925.

[42] A. Bicchi, "On the closure properties of robotic grasping," *Int. J. Robot. Res.*, vol. 14, no. 4, pp. 319–334, 1995, doi: 10.1177/027836499501400402.

[43] M. Pfanne, M. Chalon, F. Stulp, and A. Albu-Schäffer, "Fusing joint measurements and visual features for in-hand object pose estimation," *IEEE Robot. Autom. Lett.*, vol. 3, no. 4, pp. 3497–3504, Oct. 2018, doi: 10.1109/LRA.2018.2853652.

[44] M. Pfanne, M. Chalon, F. Stulp, H. Ritter, and A. Albu-Schäffer, "Object-level impedance control for dexterous in-hand manipulation," *IEEE Robot. Autom. Lett.*, vol. 5, no. 2, pp. 2987–2994, Apr. 2020, doi: 10.1109/LRA.2020.2974702.

[45] H. J. Ferreau, H. G. Bock, and M. Diehl, "An online active set strategy to overcome the limitations of explicit MPC," *Int. J. Robust Nonlinear Control, IFAC-Affiliated J.*, vol. 18, no. 8, pp. 816–830, 2008, doi: 10.1002/rnc.1251.

[46] R. M. Murray, Z. Li, and S. S. Sastry, *A Mathematical Introduction to Robotic Manipulation*. Boca Raton, FL, USA: CRC Press, 2017.

[47] C. Eppner et al., "Four aspects of building robotic systems: Lessons from the Amazon Picking Challenge 2015," *Auton. Robots*, vol. 42, no. 7, pp. 1459–1475, 2018, doi: 10.1007/s10514-018-9761-2.

“THE ANTHROPOMORPHIC LIGHTWEIGHT SYSTEM NEODAVID IS A RESEARCH ROBOT DESIGNED TO SOLVE COMPLEX MANIPULATION TASKS IN UNSTRUCTURED ENVIRONMENTS.”

“THE PRESENT VERSION OF THE UPPER BODY OF NEODAVID CONSISTS OF 173 POSITION SENSORS, THREE FORCE SENSORS, AND 83 MOTORS.”

“MECHANICAL ROBUSTNESS AGAINST IMPACTS DURING OPERATION IS ONE OF THE MAIN MOTIVATIONS FOR THE DEVELOPMENT OF NEODAVID.”

“THE CONSTRAINTS IN SIZE AND SHAPE, AS WELL AS THE VARIOUS RESEARCH GOALS ON NEODAVID, REQUIRE A WELL-STRUCTURED SYSTEM ARCHITECTURE.”

“PROPRIOCEPTION ALLOWS NEODAVID TO COPE WITH THE CHALLENGE IN TRACKING OBJECTS THAT MIGHT GET LOST DUE TO FAST MOTIONS AND LARGE OCCLUSIONS.”

“THANKS TO ITS ANTHROPOMORPHIC MULTIFINGERED HAND DESIGN, THE DLR ROBOT NEODAVID IS KINEMATICALLY CAPABLE OF PERFORMING OBJECT GRASPING AS WELL AS IN-HAND MANIPULATION TASKS.”